IET Electric Power Applications, 2021

Terminal Characteristics Measurements and Analysis of the Three-Phase Active Front End Converter Bulding Block

M. Petkovic and D. Dujic

POWER ELECTRONICS LABORATORY
ÉCOLE POLYTECHNIQUE FÉDÉRALE DE LAUSANNE

IET Research Journals

Submission Template for IET Research Journal Papers

IET Journals
The Institution of Engineering and Technology

Terminal Characteristics Measurements and Analysis of the Three-Phase Active Front End Converter Building Block

ISSN 1751-8644
doi: 0000000000
www.ietdl.org

Marko Petković and Dražen Dujić*

Power Electronics Laboratory, École Polytechnique Fédérale de Lausanne (EPFL), Lausanne, Switzerland
** E-mail: marko.petkovic@epfl.ch*

Abstract: The safe and reliable operation of modern power system imposes the need to describe and estimate the system stability through impedance-admittance measurement and identification. The integration and operation of medium voltage equipment in existing infrastructure requires impedance-admittance measurement devices which are currently few in numbers and often limited in output voltage level and output bandwidth. The four-quadrant Cascaded H-Bridge topology, featuring a three-phase Active Front End and a single-phase H-Bridge inverter presents itself as a potential solution to this problem. To support the development of the Cascaded H-Bridge topology the Active Front End hardware and control platforms require implementation and testing. The testing aspect of the process additionally includes the measurement of terminal characteristics such as the input admittance and the output impedance. The complexity of the Cascaded H-Bridge converter and its increased number of power electronics building blocks requires the use of industrial control platforms. This paper defines the hardware implementation and control principle of the three-phase Active Front End of a Cascaded H-Bridge converter as well as the system for measuring its terminal characteristics. The results obtained show that the proposed system can be successfully used to measure the input admittance and output impedance of the Active Front End upon which the development of the Cascaded H-Bridge is based.

1 Introduction

The energy demand growth in combination with the advancement in design and performance of power electronics converters has resulted in putting into service renewable energy systems as well as, extensive installation of power conversion equipment. Furthermore, apart from the ac and high voltage dc (HVdc) used for energy distribution and transport, the potential of the medium voltage dc (MVdc) systems has been thoroughly analysed, however, there are no commercial solutions nor the standards yet available [1–5]. Owing to the complexity of the installations, modelling the medium voltage (MV) systems with all of its elements is becoming increasingly challenging. A more interesting and straightforward method would be to measure the impedance or the admittance at an arbitrary interface in the network. Knowledge of the impedance or the admittance of the system and its future elements would reduce the risk of encountering unpredictable behaviour which would, in turn, provide a stable network with uninterrupted operation.

However, the problem of high-power and MV impedance and admittance measurement and the system identification still remains and there is a lack of equipment capable of performing such measurements. One of the reasons is the fact that the measurements in MV applications are not straightforward as there is a need for a device capable of operating at an MV level and injecting a perturbation into an MV system with a sufficient precision. At the same time having wide measurement bandwidth is sought after which is not easily achieved at MV level. The research performed in this field is scarce and the devices developed for that purpose are few. Medium voltage impedance/admittance measurement devices that exist today have been presented in [6–9]. These solutions have either limited bandwidth, up to $1\,\mathrm{kHz}$ or comprise an output side transformer in order to step-up the voltage to the MV levels. This in turn also limits the output bandwidth. Certain MV impedance measurement devices such as the one presented in [6] are intended for single-phase perturbation injection thus giving rise to an unbalanced system response and the presence of unwanted sideband harmonics in the frequency domain when extracting the impedance. In [10] due to the implemented control algorithm this device can inject either single-tone components or a very limited number of components at the same time, thus requiring more time to perform the impedance measurement. One of the possible solutions for the prolonged time of measurement is the usage of wideband signals [11, 12]. Still, the demand for the MV measurement equipment is growing due to the need to support the development of recent MVdc and already established medium voltage ac (MVac) applications, grid integration of renewable energy sources and storage devices, energy transmission and distribution in the MV range and ensure safe integration with the existing apparatus. Recent research focusing on the identification of impedance footprint of renewable energy sources such as wind farms has been presented in [13, 14], showing that there is a need for the measurement devices that could serve the needs of these systems.

One of the topologies capable of having sufficiently high voltage output and bandwidth is the Cascaded H-Bridge (CHB) topology with an Active Front End (AFE) interfaced to a multi-winding transformer (MWT) on the converter input side and a string of connected H-bridges (HBs) on the output side. This topology was already presented in [15], where the feasibility of using a multilevel topology for perturbation injection was studied. A high-frequency signal was superimposed to a fundamental component in open-loop and the admittance of a passive load was measured. The CHB topology presented in [15] enables a bidirectional power flow allowing the impedance or admittance measurement of various devices under test (DUTs) operating in different conditions. These capablites make the CHB topology ideal for measurement of impedances and admittances of MV systems.

The first step in development of the MV-CHB is the hardware and control implementation of the input AFE of a power electronics building block (PEBB) of the MV-CHB. Additionally, to support the hardware and control development a testing and measurement platform for the identification of the input admittance and the output impedance of the AFE is presented, where the measurement platform makes use of small-signal wideband voltage perturbation injection. For this purpose an experimental setup is assembled and presented. The system presented here includes industrial controllers and components and the direct impedance measurement is needed. The theoretical developments are out of the scope of this paper and

they can be found in more detail in [16–18]. Modelling and predicting the impedance of large systems is next to impossible due to the ever changing nature of the system and constant inclusion of new devices and power converters as well as due to the limited information about the converters given by the manufacturers. In this case, the direct measurement is the only sensible way of obtaining an impedance of a system.

The reason for development of a measurement platform is the fact that despite the MV-CHB presenting itself as a potential solution for this problem it still acts as a perturbation injection converter (PIC) for an MV system. On one side, owing to the fact that the CHB topology is supplied from another MVac system the converter requires the understanding and an assessment of its terminal characteristics for proper and safe operation. First step in characterizing the CHB converter is by acquiring the knowledge of the input admittance of its cells, i.e. the input admittance of the AFE. On the other side, the AFE and the HB need to be decoupled and the AFE should not limit the output bandwidth of the HB stage. The element linking the two converters is the output impedance of the AFE [19].

The key contributions of the work presented here are:

- Hardware development of the three-phase AFE and control platform implementation of the AFE based on a large-scale industrial control platform.
- Implementation of a standalone system for input admittance and output impedance measurement of the AFE intended to support further CHB converter cell development.
- Experimental measurement of the output impedance required for source-affected characterization of the MV-CHB PEBB [19].

The rest of the paper is organized as follows. Section II presents the CHB converter and the AFE control concept, Section III presents the terminal characteristics measurement system, Section IV presents the measurement process and results using wideband signal perturbation injection while the Section V draws conclusions.

2 Medium Voltage Cascaded H-Bridge Converter

The MV–CHB converter topology consisting of a step-down MV–MWT with 15 secondary phase-shifted outputs and 15 low-voltage cells is presented in Fig. 1. The nominal parameters of this topology, such as current and voltage ratings, as well as the grid synchronization and modulation strategies have already been presented in [15, 19, 20]. Each PEBB, presented in Fig. 2, comprises an input filter, a three-phase AFE, a dc-link capacitor and a single-phase HB. The main advantages of the CHB are the MV output voltage level and high output voltage bandwidth and thus higher frequency voltage perturbation injection and subsequently measurements obtainable in higher frequency range than was the case so far.

2.1 Active Front End

A single, ideal, AFE is presented in Fig. 3 where the output inverter from Fig. 2 is replaced by a load. Here the AFE can be regarded as a grid-connected converter as in essence it is connected to an MV grid through the MWT transformer. Considering the size and the complexity of the system, i.e. the MV–CHB converter being formed of 15 low-voltage cells, the converter control concept requires a platform capable of supporting demanding computational power and increased number of different inputs and outputs (I/Os). Usually, large-scale industrial control platforms are capable of handling such requirements. For the control of the input side of the CHB, i.e. the AFEs, the ABB AC 800PEC control system is employed together with its peripheral units for various measurements and auxiliary functions. On the other side, the task of driving the IGBT switches of the AFE is performed by the PEC gate driver unit (PEC-GDU) with intelligent functions deployed on an FPGA platform such as dc-link voltage and input currents sensing and filtering and integrated protection functions such as over-voltage and over-current protection and short-circuit protection.

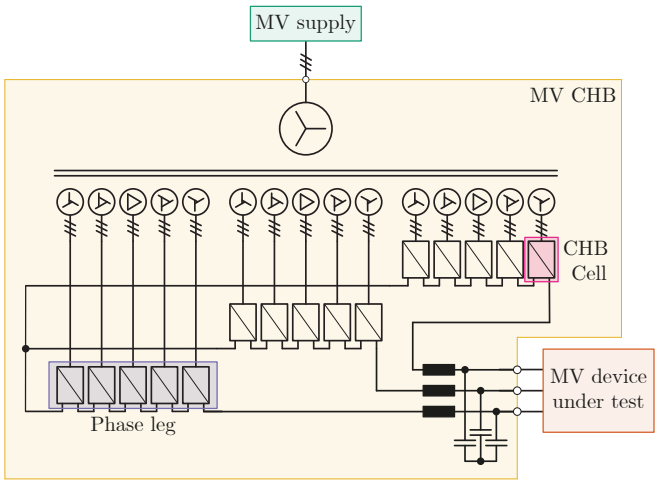

Fig. 1: Medium voltage Cascaded H-Bridge converter for perturbation injection and impedance measurement.

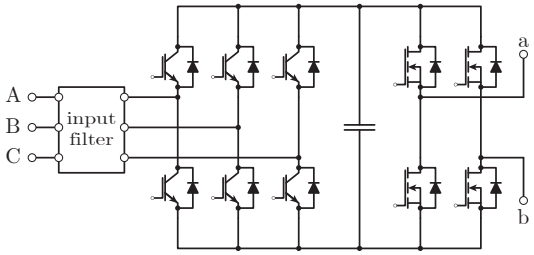

Fig. 2: MV-CHB PEBB with the input filter and the AFE stage (left) and the inverter HB stage (right).

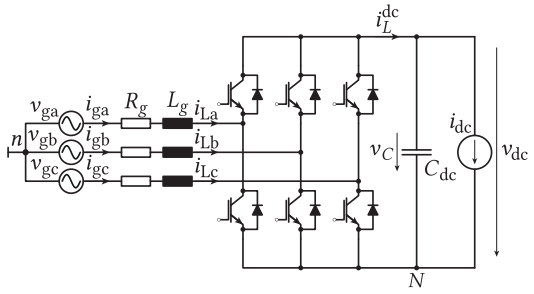

Fig. 3: Ideal three-phase AFE feeding a load, CHB in reality, and being supplied from the secondaries of the MWT.

The fact that the AFE is a grid-connected converter requires that the control structure of the AFE comprises a phase-locked loop (PLL) performing synchronization to the primary side of the transformer [21]. The dc-link voltage control (DVC), performed using a proportional integral (PI) regulator, provides the active current reference, $i_d^\star$, for the input current control (ICC), while the reactive current reference, $i_q^\star$ is set independently. The current control is implemented using the synchronous reference frame (SRF) decoupled control after which the voltage references from the *dq*-frame are transformed into the *abc*-frame references. Finally, the modulation indices for the switching legs of the AFE are sent to the PEC-GDU. The control concept can be summarized using Fig. 4. The back-to-back AFE setup with the PEC-GDU and the dc-link capacitors is presented in Fig. 5 while the AC800 PEC is presented in **??**.

The dc-link voltage references and systems commands are issued from the command and supervisory unit (CSU), essentially a human user interface, with which the AC 800PEC continuously communicates, while simultaneously exchanging information with its peripheral units and the PEC-GDU. There exist two sources of measurements required for control tasks in the AC 800PEC. First source

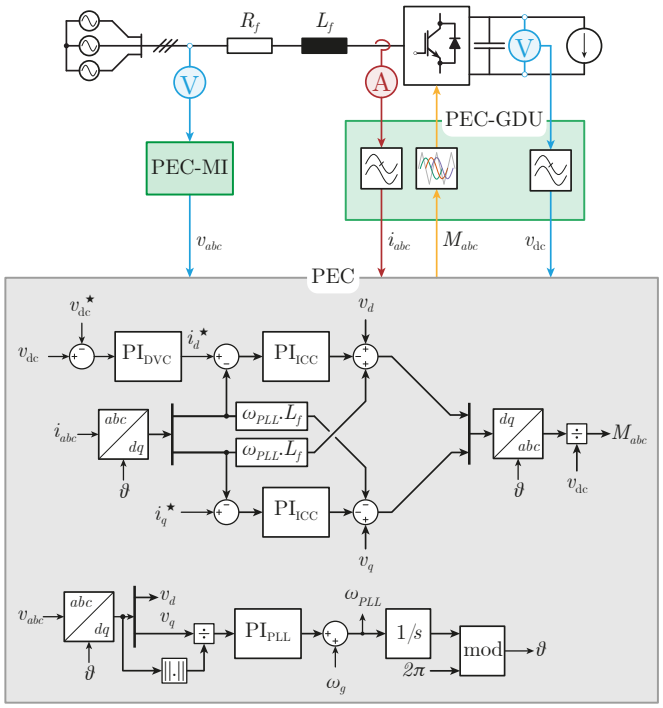

Fig. 4: Control system with where the grid synchronization, dc-link voltage and input current regulation are implemented on the AC800 PEC and the IGBT switches are driven from the PEC-GDU.

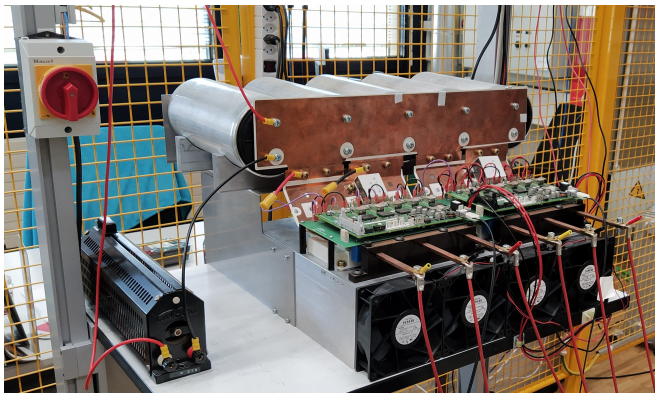

Fig. 5: Back-to-back Active Front End setup with the GDUs and the dc-link capacitor.

is the PEC measurement interface (PEC-MI), which provide the ac voltage measurements required for the grid synchronization. The second source is the PEC-GDU which provides the measurement of the dc-link voltage and the input current. Both the dc-link voltage and the current are passed either through a moving average filter or a low-pass filter in order to reduce the control sensitivity to noise and sensor imprecision. Each unit in the control structure has its own execution time which are added on top of the communication time between the PEC and its peripheral units. These times combined act as delay in the control system and affect the overall performance of the implemented control and they need to be properly compensated.

2.2 Control Tuning

The PI regulator gains of the PLL can be set using the closed loop transfer function of the PLL given as:

$$\begin{aligned} H_{CL,PLL}(s) &= \frac{K_{p,PLL}s + \frac{K_{p,PLL}}{T_{i,PLL}}}{s^2 + K_{p,PLL}s + \frac{K_{p,PLL}}{T_{i,PLL}}} \\ &= \frac{2\xi\omega_n s + \omega_n^2}{s^2 + 2\xi\omega_n s + \omega_n^2} \end{aligned} \tag{1}$$

Subsequently the gains are obtained according to the sought settling time of the second-order system which is approximated as:

$$t_s = 4.6\tau \qquad \tau = \frac{1}{\xi\omega_n} \tag{2}$$

From here, the PI controller gains can be set as a function of the settling time as follows:

$$K_{p,PLL} = 2 \cdot \xi\omega_n = \frac{9.2}{t_s} \qquad T_{i,PLL} = \frac{2\xi}{\omega_n} = \frac{t_s\xi^2}{2.3} \tag{3}$$

The damping factor is chosen as $\xi = \frac{1}{\sqrt{2}}$ while the settling time is $t_s = 100\,\mathrm{ms}$ [22].

For both the DVC and the ICC the PI regulator is taken as a regulator structure. The regulator parameters are tuned according to Magnitude Optimum for the ICC and according to Symmetrical Optimum for the DVC [23–25]. The ICC is tuned according to the following equations:

$$\begin{aligned} T_{n,ICC} &= \frac{L_f}{R_f} \\ T_{i,ICC} &= \frac{2 \cdot T_{p\Sigma,ICC}}{R_f} \\ K_{p,ICC} &= \frac{T_{n,ICC}}{T_{i,ICC}} \\ K_{i,ICC} &= \frac{1}{T_{i,ICC}} \end{aligned} \tag{4}$$

Where the $T_{p\Sigma,ICC}$ is the total delay of the ICC loop which can be established according to the switching and sampling frequencies and communication delays between the PEC and PECMI and GDU. The tuning of the DVC is performed according to the following equations:

$$\begin{aligned} T_{\Sigma,DVC} &= 10 \cdot T_{p\Sigma,ICC} \\ T_{p\Sigma,DVC} &= 2 \cdot T_{p\Sigma,ICC} + T_{\Sigma,DVC} \\ T_{n,DVC} &= 4 \cdot T_{p\Sigma,DVC} \\ T_{i,DVC} &= \frac{8 \cdot T_{p\Sigma,DVC}^2}{C_{\mathrm{dc}}} \\ K_{p,DVC} &= \frac{T_{n,ICC}}{T_{i,ICC}} \\ K_{i,DVC} &= \frac{1}{T_{i,ICC}} \end{aligned} \tag{5}$$

Where the $T_{p\Sigma,DVC}$ is the total delay of the DVC loop. The total delay of the ICC loop is be given as:

$$T_{p\Sigma,ICC} = 2 \cdot T_{GD} + 2 \cdot T_{comm} + T_{PEC} + T_{PWM} \tag{6}$$

Where the different delays and their time durations are:

- T_{GD} - gate driver ADC and calculation time $\rightarrow$ 25 µs

- T_{comm} - communication delay between the GDU and PEC $\rightarrow$ 25 µs
- T_{PEC} - ICC task calculation time $\rightarrow$ 125 µs
- T_{PWM} - PWM delay $\rightarrow$ 32.5 µs

The responses of the control system to step changes of dc-link voltage reference, output load and q-axis current reference $i_q^\star$ are given in Fig. 6. The PI regulator parameters were tuned with the following parameters, $L_f = 5\,\mathrm{mH}$, $R_f = 100\,\mathrm{m\Omega}$ and $C_{\mathrm{dc}} = 5\,\mathrm{mF}$. To test DVC, the AFE dc-link is passively charged to $v_{\mathrm{dc}} = 565\,\mathrm{V}$ after which the reference is set to $v_{\mathrm{dc}}^\star = 750\,\mathrm{V}$. From Fig. 6a it is visible that the steady-state and the issued voltage reference are reached in about 100 ms, which is due to the regulator output limits which need to be set low in the first phase of the operation of the converter, i.e. after the dc-link is charged actively. The ICC is tested by stepping the output load and maintaining the $i_q^\star = 0\,\mathrm{A}$ which influences only the d-axis regulator. It should be remarked from Fig. 6b that in this test the sudden change in the output load causes a drop in the dc-link voltage to which the DVC reacts by increasing the $i_d^\star$ and that the ICC itself does present an overshoot which can be seen in Fig. 6c where at $t = 50\,\mathrm{ms}$ the $i_q^\star$ is set at $i_q^\star = 10\,\mathrm{A}$ to test the response of the q-axis regulator. The ICC regulator performance can be evaluated from Fig. 6c where it can be seen that the newly issued reference is reached at $t = 70\,\mathrm{ms}$, i.e. the steady-state is achieved in 20 ms, showing exceptionally good tracking performance of the regulators. However, a downside of the implemented control is the absence of the disturbance compensation which is visible from the Fig. 6b. On the other side, for the disturbance compensation to be implemented another current sensor measuring the load current would need to be added to the system which would in turn increase the system cost. As for the sought for application, i.e. impedance measurement, the disturbance compensation is not a priority in the control system, this does not possess an important issue.

3 Terminal Characteristics Measurement System

The measurement of terminal characteristics of the AFE, i.e. the input admittance and output impedance, requires a system consisting of several components and is represented using the schematic in Fig. 7. Since the admittance is the ac-side characteristics in this particular case while the impedance is the dc-side the methods in which the measurements are performed are somewhat different. For the measurement of the input admittance the first component needed is a device capable of injecting small-signal voltage perturbations at the ac or the dc terminals of the AFE. A grid emulator such as Regatron TC.ACS, presented as the ACS source in Fig. 7, is capable of supplying the fundamental voltage and injecting the perturbation on top of the fundamental component and is chosen as a PIC [26]. The same grid emulator can be used as a dc source and can be used to inject small-signal perturbations. The second part of the system are the current and voltage transducers measuring the input voltage and its small signal components and the current resulting as a response of the AFE control system. The following element of the system is a high sample rate data acquisition (DAQ) instrument, presented as DAQ block in Fig. 7, collecting the measured voltages and currents for further processing. Finally, once collected, different frequency component extraction techniques can be applied to the measured voltages and currents from which the admittance and impedance can be calculated using MATLAB software in the CSU in Fig. 7.

3.1 Grid Emulator and Perturbation Injection Converter

Measuring the terminal characteristics of a grid connected converter is performed by injecting a small-signal voltage or current perturbations and measuring the resulting current or voltage response. The Regatron TC.ACS is capable of emulating an ac grid and acting as a dc voltage source and at the same time injecting small signal perturbations. Since the perturbation signals are not usually readily available in the grid emulator control software, another external signal generator is needed in order to provide references and drive the TC.ACS. For this role, the Plexim RT-Box is chosen as a versatile device that can perform the duty of the signal generator. In the RT-Box the ac grid and dc voltage source models are established and its analog outputs are used as the analog inputs for the Regatron TC.ACS output voltage references.

Measuring the input admittance is performed by injecting small signal voltage perturbation in the output voltage reference of the TC.ACS. These perturbations give rise to current response as a consequence of the AFE control system upon which the ac-side voltage and current measurements are collected.

On the other hand, measuring the output impedance can either be performed having a controllable current source or combining a controllable voltage source with an inductor or a resistor in series. The TC.ACS combined with the resistor R_{dc} acts as a controllable current source. By controlling the output voltage of the TC.ACS and injecting small signal perturbations in this voltage a current perturbation for the AFE is created. This provokes a response from the AFE dc-link voltage control after which the dc-side voltage and current measurements are collected.

3.2 Perturbation Signal

Widely popular method in impedance/admittance measurements is the sine sweep, which requires one by one frequency small-signal perturbation injection and collection of response, thus requiring large number of measurements and time to be executed. If the measurement time is too long, the measured object may as well be disturbed and change its operating point and subsequently the impedance or admittance would change. This is somewhat improved with multi-tone signals but the energy of this signal is reduced with the number of tones it consists of. Recently, pseudo-random

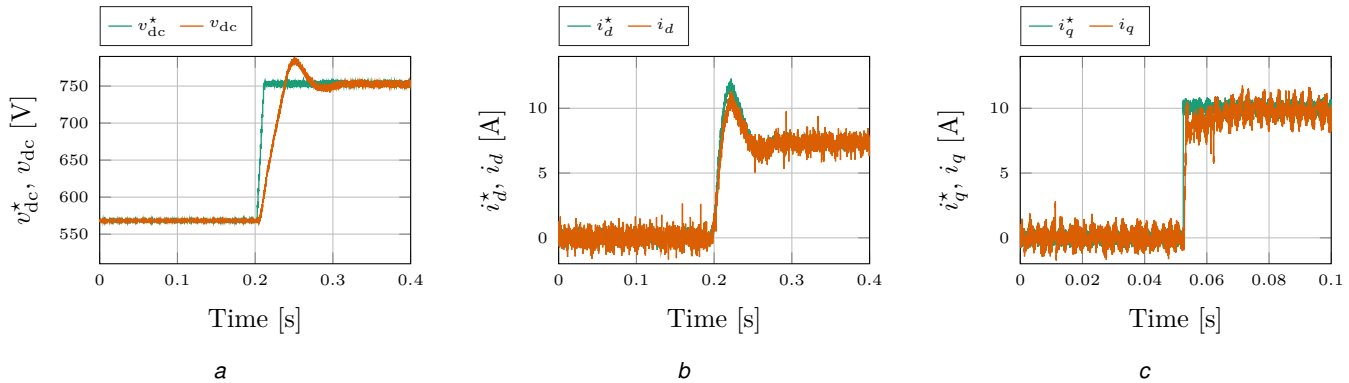

Fig. 6: Voltage and current response waveforms for the step change of **a)** the dc-link voltage reference, **b)** the output load and **c)** the q-axis current.

binary sequence (PRBS) signals (c.f. Fig. 8) have seen substantial use for system identification and impedance measurement [27–29]. The advantage of these signals lies in the fact that they are well suited for the characterization of dynamics systems where rapid measurement is necessary due to the possibility of variation of the system state in time. The maximum frequency of the perturbation signals needs to be chosen with respect to PIC output bandwidth as well as the DUT switching frequency, thus some preliminary knowledge of the DUT parameters is needed. In this particular case, the PRBS-9 signal is used resulting in a 511-bit-long signal (c.f. Fig. 10). Taking into account the Regatron ACS output voltage control bandwidth, the sequence was generated at $f_{\text{gen}} = 2\,\text{kHz}$, which sets the injection time at about $t_p = 250\,\text{ms}$ and the resolution frequency at $f_{\text{res}} = 3.914\,\text{Hz}$. For the sake of comparison between the PRBS and ac sweep injection the following analysis can be performed. Performing an ac sweep with 511 different frequencies which are given as $f_p = 3.914, 2 \cdot 3.914, 3 \cdot 3.914, \ldots, 2000\,\text{Hz}$ and performing 16 injections yields the total injection time of $t_{\text{sweep}} = 27.85\,\text{s}$. Performing the same perturbation injection with the PRBS signal yields the total time of $t_{\text{PRBS}} = 4.088\,\text{s}$. Thus, performing the ac sweep injection in this particular case takes seven times longer. Moreover, when performing the frequency analysis and frequency component extraction using the FFT methods, the ac sweep method requires that each dataset is analyzed separately and that a single frequency is extracted at a time, while with the PRBS method all of the 511 components are extracted in a single iteration. The injected PRBS-12 signal in the time domain and its frequency domain counterpart are presented in Fig. 9.

3.3 *Voltage and Current Measurement*

Even though the input admittance is represented in the *dq*-frame, the only available voltage and current measurements are in the *abc*-frame. These measurements are implemented using voltage and current transducers. The issue of choice of transducers lies in the fact that they need to be able to measure the nominal voltage and current values of the system while at the same time being able to measure the small-signal portion of the measurand with a good enough precision. Moreover, depending on the choice of the PRBS type signal and its generation frequency, the perturbation signal may often have high frequency components which in turn requires that the transducers chosen have a large enough bandwidth for the measurement. Likewise, the PRBS signals contain low-frequency components resulting in the need that the transducers need to reliably measure the low-frequency signals. The sensors chosen for the voltage and current measurements are the ABB VS1500B and LEM LF210-S transducers, respectively. In total, there are six sensors, three for voltage and three for currents. Since the neutral point is available at the output terminals of the Regatron ACS, the line-to-neutral voltages and line currents are measured. When measuring the output impedance the same transducers can be used, however this time measuring the dc-link voltage of the AFE and the output, or load, current. In order to interface the transducer output to the DAQ system an intermediate board is added to the system that simultaneously incorporates a $f_c = 10\,\text{kHz}$ low-pass analog filter and voltage limiters in order not to damage the DAQ system.

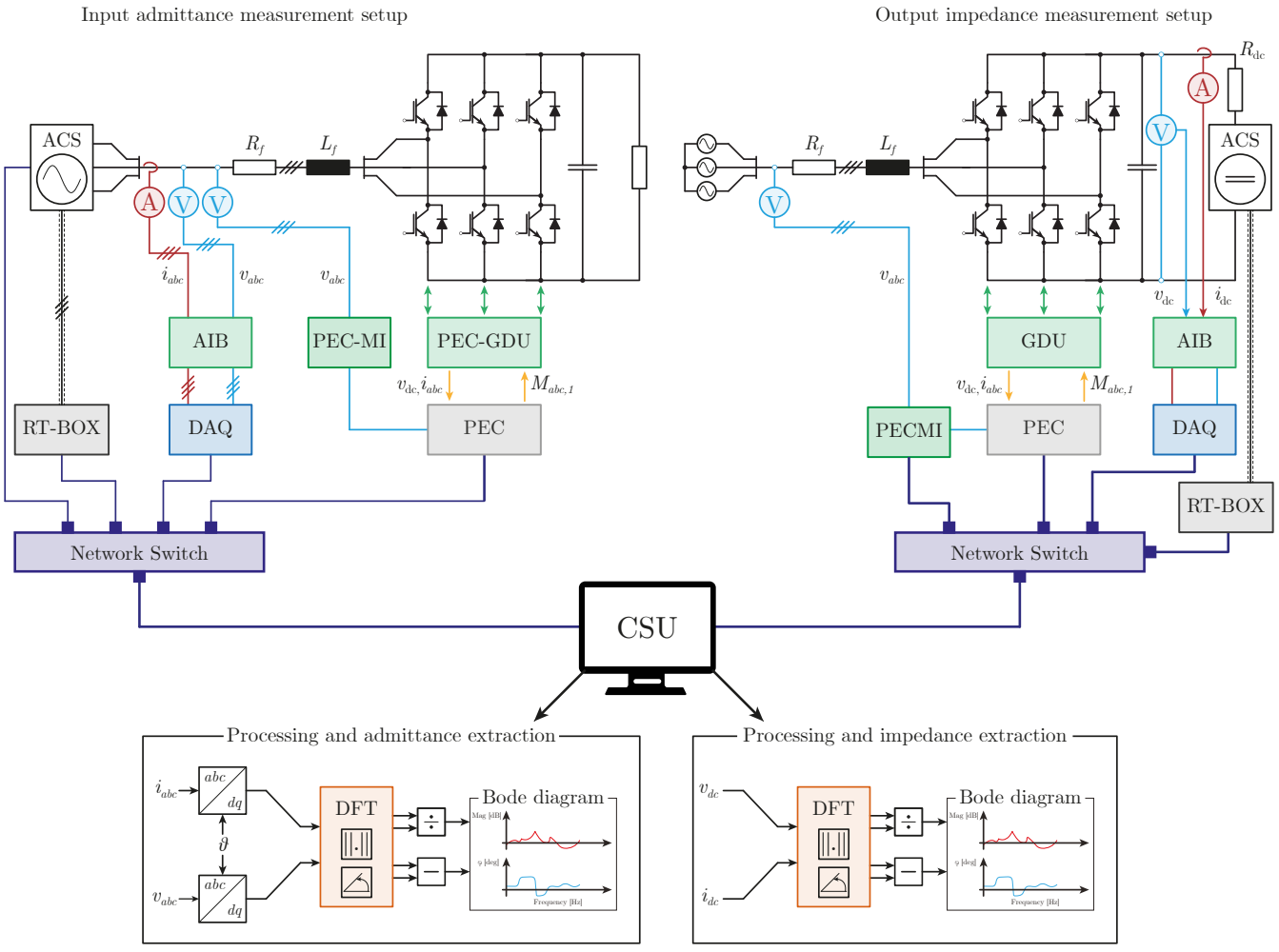

Fig. 7: Schematics of the experimental setup for the measurement of the input admittance and the output impedance of the AFE.

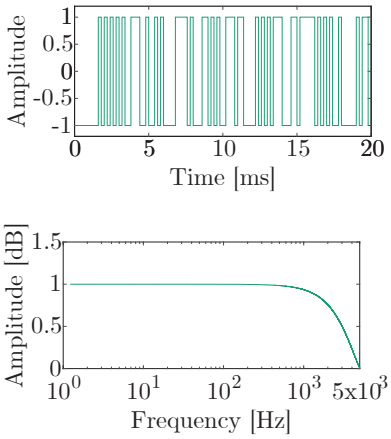

Fig. 8: PRBS-12 signal in time and frequency domain.

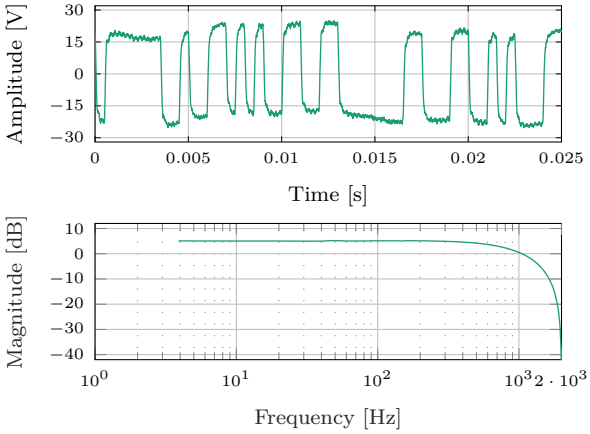

Fig. 9: The injected and measured PRBS-12 signal in time and frequency domain.

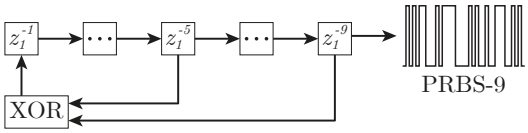

Fig. 10: Shift register circuit for PRBS generation.

3.4 Data Acquisition System

In order to follow up with the requirements for having high-bandwidth, precise voltage and current transducers for measurements the DAQ system employed needs to have a high sampling rate as well. Due to the number of signals acquired the sampling of each signal needs to be performed simultaneously in order to avoid delays between the signals sampled. Furthermore, having a system capable of storing large amounts of data, namely more than one perturbation period is sought for. The reason for this is the fact that having multiple periods measured and acquired allows for averaging over these multiple periods. This greatly improves the quality of results in systems where unwanted noise is unavoidably present. A DAQ fulfilling these requirements is the Elsys Tranet 408s transient recorder capable of performing sampling at a rate of up to $M = 80\,\mathrm{MS\,s^{-1}}$. The voltage and current measurements are acquired over a time period of about $t_r = 4\,\mathrm{s}$ which, taking into account the resolution frequency, leads to 16 perturbation periods acquired.

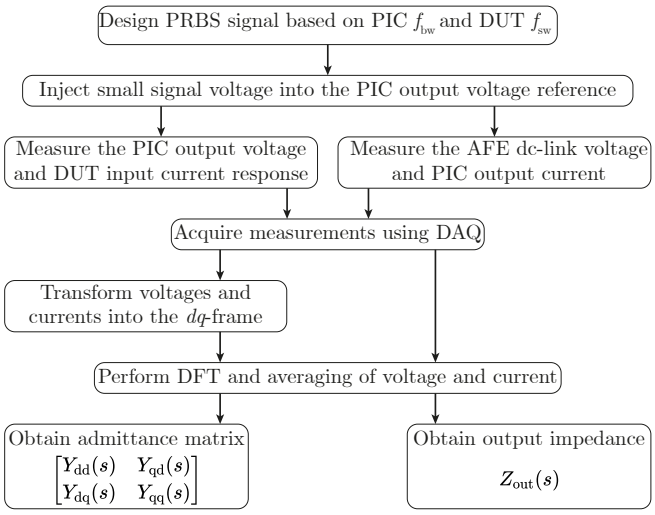

Fig. 11: Flowchart for input admittance and output impedance measurement of the AFE.

3.5 Admittance and Impedance Extraction

Once measured and collected with the DAQ, the voltage and current measurement can be used for processing. In this particular case this is done offline using MATLAB software. In order to extract the frequency components, namely magnitude and phase, from the measurements the discrete Fourier transform (DFT) is performed. The acquired data is split into 16 periods of identical length and the DFT is performed on these periods upon which the data are averaged. Here, the geometric mean is used to average the measurements which is given as:

$$\bar{x} = \left(\prod_{i=1}^{n} x_i \right)^{\frac{1}{n}} \tag{7}$$

Where the x is the voltage or current measurement and $i = 1, 2, \ldots, 16$ denoting the i^{th} period of the data.

Following the averaging of the data the admittance matrix in the dq-frame is extracted as:

$$\begin{aligned} \mathbf{Y}_{\text{in}}(s) &= \begin{bmatrix} i_{d,1}(s) & i_{d,2}(s) \\ i_{q,1}(s) & i_{q,2}(s) \end{bmatrix} \cdot \begin{bmatrix} v_{d,1}(s) & v_{d,2}(s) \\ v_{q,1}(s) & v_{q,2}(s) \end{bmatrix}^{-1} \\ &= \begin{bmatrix} Y_{\text{dd}}(s) & Y_{\text{dq}}(s) \\ Y_{\text{qd}}(s) & Y_{\text{qq}}(s) \end{bmatrix} \end{aligned} \tag{8}$$

Where the $i_{x,y}$ and $v_{x,y}$ are the measured currents and voltage in the dq-frame after the first and second injection. Similarly, the DFT is performed on the dc-side voltage and current measurements and the output impedance can be extracted as:

$$Z_{\text{out}}(s) = \frac{\left\|\tilde{v}(s)\right\|}{\left\|\tilde{i}(s)\right\|} \left[\angle\tilde{v}(s) - \angle\tilde{i}(s) \right] \tag{9}$$

The admittance and impedance measurement method can be summarized using the flowchart presented in Fig. 11.

4 Measurement Results

The implemented experimental setup for the ac-side input admittance measurement using the elements outlined is presented in Fig. 12 while for the setup for the measurement of the dc-side output impedance one can refer itself to the right hand side of Fig. 7. The same elements from Fig. 12 are reused for output impedance

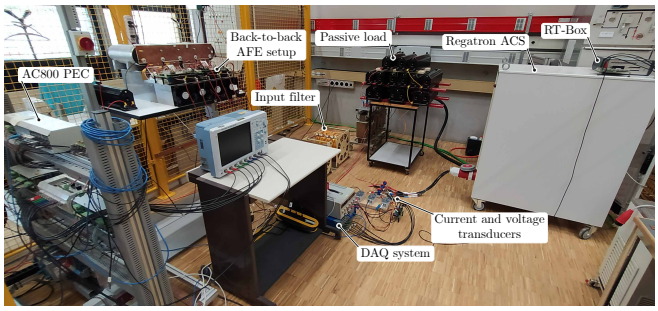

Fig. 12: Experimental setup for the input admittance and output impedance measurement including the RT-Box driving TC.ACS employed as a PIC, the input L-type filter, the AC800 PEC controller, back-to-back AFE setup and the passive load.

Table 1 System parameters for input admittance measurements

Measurement	I	II	III	IV
$K_{p,ICC}$	9.43	9.43	7.1	5.1
$K_{i,ICC}$	118.7	118.7	141.5	94.4
$K_{p,DVC}$	0.8	0.8	0.6	0.8
$K_{i,DVC}$	61.8	61.8	34.8	61.8
$K_{p,PLL}$	92	92	92	92
$K_{i,PLL}$	4232	4232	4232	4232
P_{in}	22 kW	11 kW	22 kW	22 kW
L_f	5 mH	5 mH	5 mH	2.7 mH
R_f	100 mΩ	100 mΩ	100 mΩ	100 mΩ
f_{sw}	8 kHz	8 kHz	6 kHz	8 kHz
C_{dc}	5 mF	5 mF	5 mF	5 mF

measurement but respecting the layout of Fig. 7. The amount of small-signal voltage injected is about 5–6 % of the nominal voltage. Even though injecting more voltage is desirable from the standpoint of obtaining better measurements, it is in turn undesirable from the perspective of the system protection, thus the level of injected voltage must be carefully chosen in order not to perturb the normal operation of the AFE.

For the admittance measurements two injections are performed, one in the d-axis of the reference voltage and the second in the q-axis. In total, four different measurements were performed in which the AFE was operating with different parameters, such as a different inductance of the input filter, a different switching frequency or a different operating point, i.e. a different value of the load. Both the value of the filter and the switching frequency influence the DVC and ICC PI regulator gains which in turn influences the shape of the admittance. In all four measurements the input line-to-line voltage was established at $v_g = 400\,\text{V}$. The reduced input voltage compared to the nominal voltage of the AFE is due to the limitations of the TC.ACS output voltage level. Different parameters of the performed measurements are summarized in Table 1.

From results presented in Figs. 13 to 16 it is noticeable that there is a difference in measured input admittance depending on the parameters from Table 1. The operating point mostly influences the low frequency region which is clearly visible by comparing Figs. 13 and 14. The difference in switching frequency alters the regulator gains and reduces the control bandwidth which is interpreted as having a slightly lower admittance in Fig. 15 and the characteristics shifting to the left in the frequency range compared to Fig. 13. Additionally, in Fig. 13 a set of measured impedances obtained using

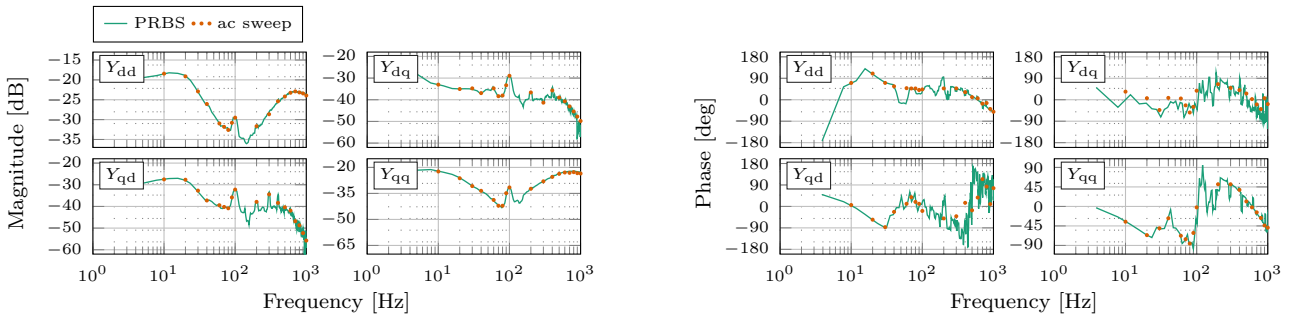

a *b*

Fig. 13: **a)** magnitude and **b)** phase of input admittance matrix $\mathbf{Y}_{\text{in}}$ of the AFE with parameters of measurement I presented in Table 1. Two sets of measurements are shown, one obtained using the PRBS injection and another, a reference set, obtained using the ac sweep injection.

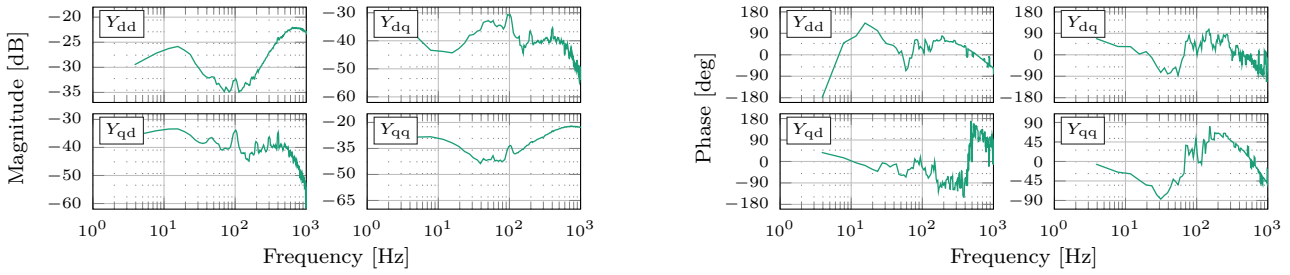

a *b*

Fig. 14: **a)** magnitude and **b)** phase of input admittance matrix $\mathbf{Y}_{\text{in}}$ of the AFE with parameters of measurement II presented in Table 1.

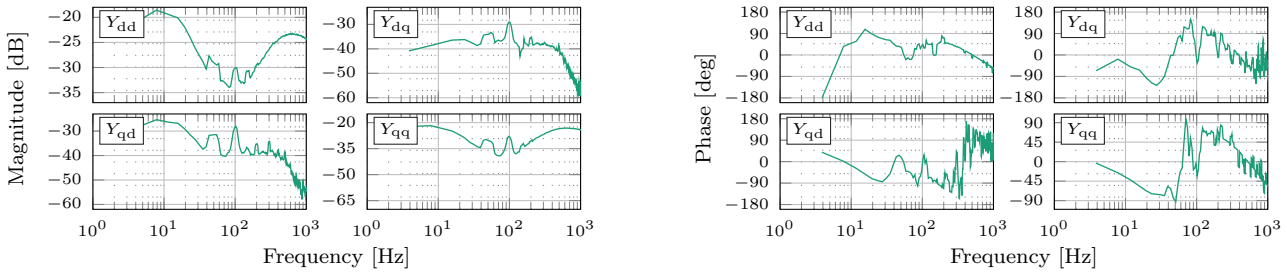

Fig. 15: **a)** magnitude and **b)** phase of input admittance matrix $\mathbf{Y}_{\text{in}}$ of the AFE with parameters of measurement III presented in Table 1.

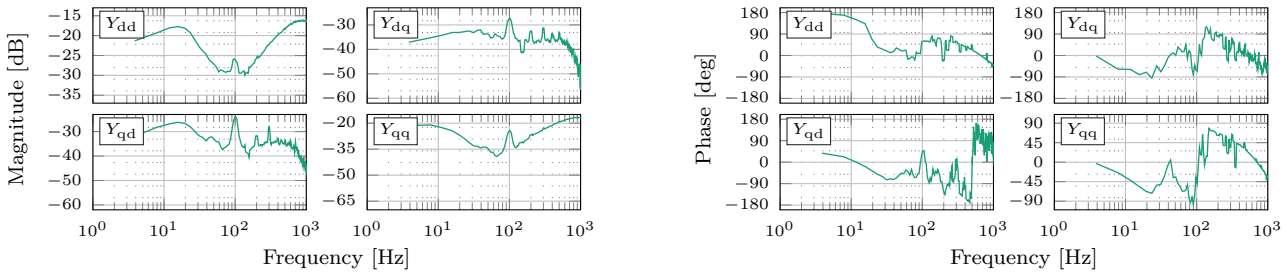

Fig. 16: **a)** magnitude and **b)** phase of input admittance matrix $\mathbf{Y}_{\text{in}}$ of the AFE with parameters of measurement IV presented in Table 1.

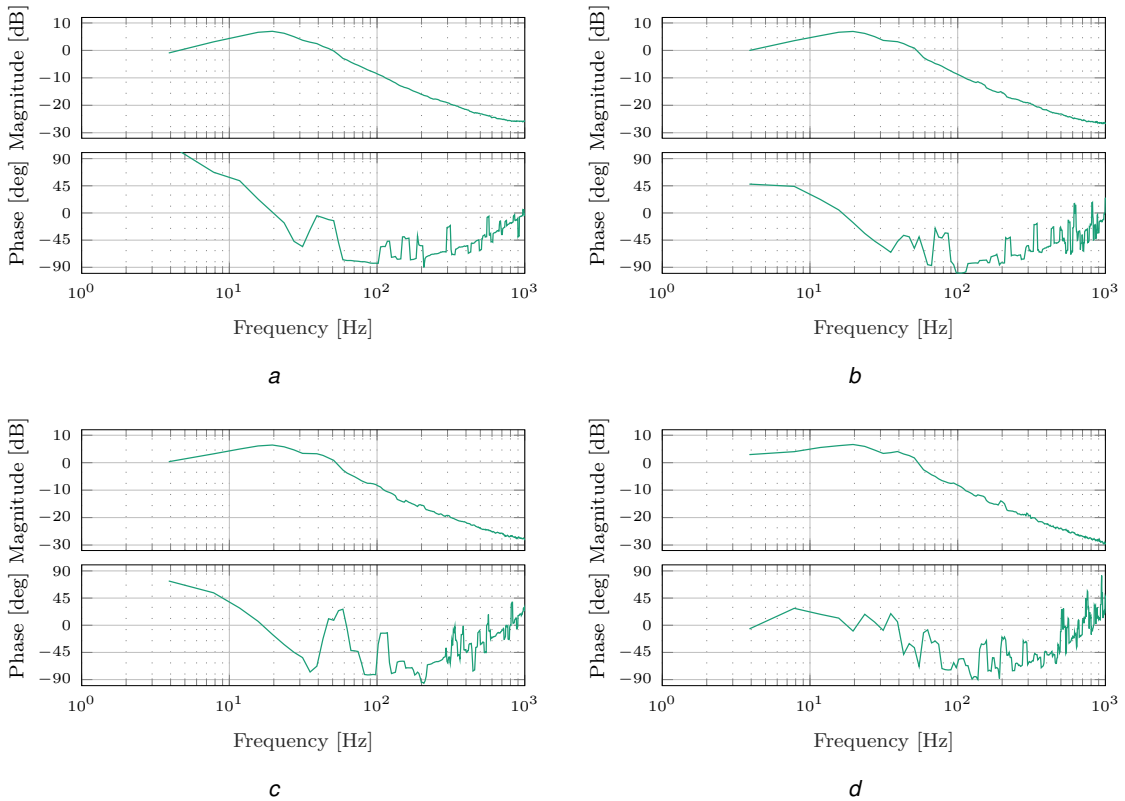

Fig. 17: Magnitude and phase of output impedance Z_{out} of the AFE with **a)** $I_{\text{dc}} = 5\,\text{A}$, **b)** $I_{\text{dc}} = 7.5\,\text{A}$, **c)** $I_{\text{dc}} = 10\,\text{A}$ and **d)** $I_{\text{dc}} = 12.5\,\text{A}$.

the ac sweep injection, which serves as a reference measurement, is added on top of the results obtained with the PRBS injection.

When it comes to the impedance measurements four different measurements were performed as well. The load current was varied between $5\,\mathrm{A}$ and $12.5\,\mathrm{A}$, resulting in the power variation between $3.75\,\mathrm{kW}$ and $9.4\,\mathrm{kW}$. The experimental measured output impedances are presented in Fig. 17 for four different loads. It can be discerned between Figs. 17a to 17d that the impedance shape or rather its value changes in the low frequency range. The variation is between $-1\,\mathrm{dB}$ and $3\,\mathrm{dB}$ which is characteristic for the change of operation point of the converter. Moreover, the impedance shape presents a drop after $20\,\mathrm{Hz}$ which indicates the bandwidth of the DVC. However, the output impedance has a highest value between the dc value and $50\,\mathrm{Hz}$ after which the impedance decreases sharply with a rate of $-25\,\mathrm{dB/dec}$. Thus it can be concluded that outside of this range, and in general, outside of the output voltage control range, the output impedance has little influence on the system. In conjunction with the results from [19] it can be concluded that the output impedance has little effect on the control-to-output characteristics of the CHB beyond $50\,\mathrm{Hz}$.

Nevertheless, the presented system does feature certain limit such as the limited frequency range in which the measurement is performed. This, however, depends on the perturbation injection device employed for the process and since it is a commercial device it is one of the drawbacks that is not solved easily. Another limitation is the fact that the measurements were performed on a system with lower ratings than the nominal ones presented in [19], which is also due to the limited output voltage of the supply source used.

5 Conclusion

This paper has presented the design and implementation of the AFE of a PEBB of the MV-CHB converter, as well as the testing and measurement platform for input admittance and output impedance measurement of the AFE. The presented results indicate that the measurement platform and methods applied can clearly distinguish different admittance shapes arising as a result of the change of parameters of the AFE. Moreover, due to the frequent lack of knowledge of all parameters of industrial equipment employed for the control of the converter, practical measurements are usually the only trustworthy method of admittance or impedance identification for power electronics converters. Furthermore, the use of wideband signals for measurements has double benefit. One benefit is the significant reduction in measurement time and complexity compared to standard methods such as an ac frequency sweep while the other one is preventing that the converter on which the measurements are performed changes operation point during the measurement. Namely, the measurement time is reduced sevenfold compared to the use of ac sweep signal injection and measurement. Moreover, the post-processing time and impedance extraction time is reduced. Presented measurement platform and results serve as a basis for proper understanding and operation of the MV-CHB as well as experimental verification of the way in which the AFE influence the HB in the MV-CHB PEBB and its output overall.

6 References

1 G. L. Kusic, G. F. Reed, J. Svensson, and Z. Wang, "A case for medium voltage DC for distribution circuit applications," in *2011 IEEE/PES Power Systems Conference and Exposition*. IEEE, 2011, pp. 1–7.

2 A. Hinz, M. Stieneker, and R. W. De Doncker, "Impact and opportunities of medium-voltage dc grids in urban railway systems," in *2016 18th European Conference on Power Electronics and Applications (EPE'16 ECCE Europe)*. IEEE, 2016, pp. 1–10.

3 U. Javaid, F. D. Freijedo, W. van der Merwe, and D. Dujic, "Stability analysis of multi-port mvdc distribution networks for all-electric ships," *IEEE Journal of Emerging and Selected Topics in Power Electronics*, vol. 8, no. 2, pp. 1164–1177, 2019.

4 M. Mogorovic and D. Dujic, "100 kW, 10 kHz medium-frequency transformer design optimization and experimental verification," *IEEE Transactions on Power Electronics*, vol. 34, no. 2, pp. 1696–1708, 2018.

5 M. Utvic, S. Milovanovic, and D. Dujic, "Flexible Medium Voltage DC Source Utilizing Series Connected Modular Multilevel Converters," in *2019 21st European Conference on Power Electronics and Applications (EPE'19 ECCE Europe)*, no. CONF, 2019.

6 M. Jakšić, Z. Shen, I. Cvetković, D. Boroyevich, R. Burgos, C. DiMarino, and F. Chen, "Medium-voltage impedance measurement unit for assessing the system stability of electric ships," *IEEE Transactions on Energy Conversion*, vol. 32, no. 2, pp. 829–841, 2017.

7 F. Hahn, S. Brüske, B. Benkendorff, G. Büticchi, F. W. Füchs, and M. Liserre, "Wide frequency range medium-voltage grid impedance analysis by current injection of a multi-MW power converter," in *2016 18th European Conference on Power Electronics and Applications (EPE'16 ECCE Europe)*. IEEE, 2016, pp. 1–10.

8 E. Ledezma, K. Wang, T. Keister, R. Edwards, R. Pipho, B. Palle, D. Kulkarni, T. E. Salem, J. C. Fox, and L. Parsa, "Development of a modular configurable multi-megawatt power amplifier," in *IECON 2013-39th Annual Conference of the IEEE Industrial Electronics Society*. IEEE, 2013, pp. 631–636.

9 F. Bogdan, J. Hauer, J. Langston, K. Schoder, M. Steurer, I. Cvetkovic, Z. Shen, M. Jaksic, C. DiMarino, F. Chen, D. Boroyevich, and R. Burgos, "Test environment for a novel medium voltage impedance measurement unit," in *2015 IEEE Electric Ship Technologies Symposium (ESTS)*, June 2015, pp. 99–103.

10 Z.-X. Zou, F. Hahn, G. Buticchi, S. Günter, and M. Liserre, "Interleaved operation of two neutral-point-clamped inverters with reduced circulating current," *IEEE Transactions on Power Electronics*, vol. 33, no. 12, pp. 10 122–10 134, 2018.

11 H. Gong, X. Wang, and D. Yang, "Dq-frame impedance measurement of three-phase converters using time-domain mimo parametric identification," *IEEE Transactions on Power Electronics*, vol. 36, no. 2, pp. 2131–2142, 2020.

12 H. Alenius, R. Luhtala, and T. Roinila, "Amplitude design of perturbation signal in frequency-domain analysis of grid-connected systems," *IFAC-PapersOnLine*, vol. 2020, pp. 1–6, 2020.

13 S. D. Shah, P. J. Koralewicz, V. Gevorgian, and R. B. Wallen, "Impedance measurement of wind turbines using a multimegawatt grid simulator," National Renewable Energy Lab.(NREL), Golden, CO (United States), Tech. Rep., 2019.

14 H. Zong, J. Lyu, X. Wang, C. Zhang, R. Zhang, and X. Cai, "Grey box aggregation modeling of wind farm for wideband oscillations analysis," *Applied Energy*, vol. 283, p. 116035, 2021.

15 M. Petković, N. Hildebrandt, F. D. Freijedo, and D. Dujić, "Cascaded H-Bridge Multilevel Converter for a High-Power Medium-Voltage Impedance-Admittance Measurement Unit," in *2018 International Symposium on Industrial Electronics (INDEL)*, Nov 2018, pp. 1–8.

16 L. Harnefors, M. Bongiorno, and S. Lundberg, "Stability analysis of converter-grid interaction using the converter input admittance," in *2007 European Conference on Power Electronics and Applications*. IEEE, 2007, pp. 1–10.

17 ——, "Input-admittance calculation and shaping for controlled voltage-source converters," *IEEE transactions on industrial electronics*, vol. 54, no. 6, pp. 3323–3334, 2007.

18 B. Wen, D. Boroyevich, R. Burgos, P. Mattavelli, and Z. Shen, "Small-signal stability analysis of three-phase AC systems in the presence of constant power loads based on measured dq frame impedances," *IEEE Transactions on Power Electronics*, vol. 30, no. 10, pp. 5952–5963, 2014.

19 M. Petković and D. Dujić, "Hardware-in-the-Loop Characterization of Source-Affected Output Characteristics of Cascaded H-Bridge Converter," *IEEE Journal of Emerging and Selected Topics in Power Electronics*, pp. 1–1, 2020.

20 N. Hildebrandt, M. Luo, and D. Dujic, "Robust and Cost Effective Synchronization Scheme for a Multicell Grid Emulator," *IEEE Transactions on Industrial Electronics*, pp. 1–1, 2020.

21 N. Hildebrandt and D. Dujic, "Supply Grid Synchronization and Operation of a Filterless Cascaded H-Bridge based Grid Emulator," in *The 45th Annual Conference of the IEEE Industrial Electronics Society-IECON 2019*, no. CONF, 2019.

22 R. Teodorescu, M. Liserre, and P. Rodriguez, *Grid Synchronization in Single Phase Power Converters*. IEEE, 2007.

23 A. Whiteley, "Theory of servo systems, with particular reference to stabilization," *Journal of the Institution of Electrical Engineers-Part II: Power Engineering*, vol. 93, no. 34, pp. 353–367, 1946.

24 W. Leonhard, "Regelkreise mit symmetrischer Ubertragungsfunktion," *at-Automatisierungstechnik*, vol. 13, no. 1-12, pp. 4–12, 1965.

25 C. Kessler, "Das Symmetrische Optimum, Teil I, Regelungstechnik 11, 6," 1958.

26 Regatron AG, *Regatron TC.ACS Full 4-Quadrant Grid Simulator Device Manual*, Regatron.

27 R. Luhtala, T. Roinila, and T. Messo, "Implementation of Real-Time Impedance-Based Stability Assessment of Grid-Connected Systems Using MIMO-Identification Techniques," *IEEE Transactions on Industry Applications*, vol. 54, no. 5, pp. 5054–5063, Sep. 2018.

28 T. Roinila, H. Abdollahi, S. Arrua, and E. Santi, "Real-Time Stability Analysis and Control of Multiconverter Systems by Using MIMO-Identification Techniques," *IEEE Transactions on Power Electronics*, vol. 34, no. 4, pp. 3948–3957, April 2019.

29 T. Roinila, T. Messo, R. Luhtala, R. Scharrenberg, E. C. W. de Jong, A. Fabian, and Y. Sun, "Hardware-in-the-Loop Methods for Real-Time Frequency-Response Measurements of on-Board Power Distribution Systems," *IEEE Transactions on Industrial Electronics*, vol. 66, no. 7, pp. 5769–5777, July 2019.